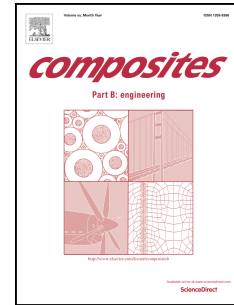


Accepted Manuscript

Glass fibre reinforced polymer composites toughened with acrylonitrile butadiene nanorubber

Nazli G. Ozdemir, Tao Zhang, Homayoun Hadavinia, Ian Aspin, Fabrizio Scarpa



PII: S1359-8368(15)00539-9

DOI: [10.1016/j.compositesb.2015.09.004](https://doi.org/10.1016/j.compositesb.2015.09.004)

Reference: JCOMB 3771

To appear in: *Composites Part B*

Received Date: 30 May 2015

Accepted Date: 10 September 2015

Please cite this article as: Ozdemir NG, Zhang T, Hadavinia H, Aspin I, Scarpa F, Glass fibre reinforced polymer composites toughened with acrylonitrile butadiene nanorubber, *Composites Part B* (2015), doi: 10.1016/j.compositesb.2015.09.004.

This is a PDF file of an unedited manuscript that has been accepted for publication. As a service to our customers we are providing this early version of the manuscript. The manuscript will undergo copyediting, typesetting, and review of the resulting proof before it is published in its final form. Please note that during the production process errors may be discovered which could affect the content, and all legal disclaimers that apply to the journal pertain.

Glass fibre reinforced polymer composites toughened with acrylonitrile butadiene nanorubber

Nazli G Ozdemir¹, Tao Zhang¹, Homayoun Hadavinia¹, Ian Aspin², Fabrizio Scarpa³

¹Kingston University London, SW15 3DW, United Kingdom

²Cytec Industrial Materials, DE75 7SP, United Kingdom

³ACCIS, University of Bristol, BS8 1TR, United Kingdom

ABSTRACT

We present the effects of nano carboxylic acrylonitrile butadiene (CNBR-NP) and nano acrylonitrile butadiene (NBR-NP) rubbers on the interlaminar shear strength, fracture toughness and Charpy impact strength of glass fibre/ dicyandiamide-cured epoxy matrix composites (GFRP). Dispersions of 20 phr of nanorubber into the matrix significantly improved the Mode I (G_{IC}) and Mode II (G_{IIC}) delamination fracture toughness of the GFRP panels by 190% and 70% respectively. No noticeable change in the glass transition temperature of the composite panels was observed. Scanning electron microscopy images of the fracture surfaces showed evidence of the existence of toughening mechanisms such as de-bonding of the nanorubber, as well as presence of crack path deflections and fibres bridging.

Keywords: A. Polymer-matrix composites (PMCs), B. Fracture toughness, D. Mechanical testing, E. Lay-up (manual)

*Corresponding Author:

Tel: +44 (0) 7450227535, E-mail address: gulsine@yahoo.com (N.G. Ozdemir)

Present Address: ACCIS, University of Bristol, BS8 1TR, United Kingdom

1. INTRODUCTION

Fibre reinforced polymers (FRP) are gaining importance in engineering applications because of their high specific strength and versatility of use. However, FRPs are also characterised by low fracture toughness because of the brittleness of their main matrix material – epoxy resins. While strength and rigidity of epoxy resins are desirable in many engineering applications, low fracture toughness limits their performance. Due to this drawback, scientists have been modifying the structure of epoxy resins with tougheners for more than 3 decades.

Dicyandiamide (DICY) cured epoxy resins are well known in industry as prepreg constituents and curable structural adhesives [1, 2, 3, 4, 5]. Solid acrylonitrile butadiene rubber (NBR) with high acrylonitrile content provides a good compatibility between the NBR and the epoxy resin [6, 7]. Carboxylic acrylonitrile butadiene rubber (CNBR) is a modified NBR with carboxylic groups along the hydrocarbon backbone, and imparts an even better compatibility with epoxy than NBR due to the presence of active polar groups on the particles surface [8]. To the best of the Authors' knowledge no previous study has been reported or published in open literature about the toughening of dicyandiamide-cured epoxy matrix with acrylonitrile-based nanorubber materials and the related mechanical properties of the resulting nanocomposites, because of the challenges in processing the materials and the complex structure and cross-linking mechanism of DICY curing agent [9]. Further research is needed in this area, and this forms the primary motivation of the current work.

A significant body of literature describes the effects on the mechanical properties of epoxy resin systems by adding nanorubber [10, 9, 8, 4, 11]. However, there is a

noticeable lack of work that illustrates the mechanical properties of FRPs with nanorubber-toughened epoxy as matrix, mainly because of the increase in the viscosity of the resin with the use of nanorubber that makes difficult the penetration of the nano-modified resin through the fibres. In this paper we also describe the analysis on GFRPs panels with the nano-rubber toughened matrix produced by hand lay-up techniques. The outcome of the hand lay-up process is not affected by viscosity changes. Moreover, a relatively high viscosity of the nano-modified matrices prevent resin leakage at high processing pressures, providing therefore improved interfacial properties. Epoxy matrices have been toughened with nanorubber using a laboratory-scale triple mill that generated particles with small sizes and dispersions with even distributions that resulted in a toughened network.

2. MATERIALS AND COMPOSITES MANUFACTURING

The epoxy resin used was liquid DGEBA (Araldite LY1556) with equivalent weight of epoxide equal to 188 (Huntsman, UK). Dicyandiamide (DICY, Dyhard D50EP) was used as the curing agent and a difunctional urone (Dyhard UR500) was used as the accelerator, both supplied by AlzChem, UK. Nano carboxylic acrylonitrile butadiene rubber (CNBR-NP) Narpow VP-501 (single particle size distribution 50-100 nm, acrylonitrile content, 26wt %), and nano acrylonitrile butadiene rubber (NBR-NP) Narpow VP-401 (single particle size distribution 100-150 nm, acrylonitrile content, 26wt %) were received as powders from SINOPEC, Beijing Research Institute of Chemical Industry (BRICI), China. Fumed silica (FS) received from Aerosil, UK ($D_{50}=1\ \mu\text{m}$) was used in some of the formulations to modify the rheological behaviour of the nanofluids to help with the GFRP laminates production. Glass plies from Sigmatex

(UK) Ltd (2x2 twill with 287GSM) have been used to produce the GFRP panels. The matrix formulations used in this work are shown in Table 1.

The nanorubber modified resin matrices were first produced by drying the nanorubber at $\sim 70^{\circ}\text{C}$ for 16 hours in an oven to eliminate the absorbed moisture. After drying, the nanorubber was dispersed in the DGEBA matrix and the blend was speed-mixed at 3500 rpm for 1 minute using a DAC 150.1 FVZ speed mixer. Fumed silica (0.25 to 1 phr, depending on the final viscosity of the blend) has been then added to the epoxy matrix in selected samples. The dispersion of the fumed silica considerably increases the viscosity of the blends and helps to prevent the leakage of the resin matrix during the curing of the GFRP laminates in autoclave under high pressures. To improve the homogeneity of the mixture, the blend was triple milled for 6 times at room temperature ($\text{RT}=23^{\circ}\text{C}$). After mixing, the blend has been magnetically stirred at a speed of 320 rpm and degassed at 70°C inside a glass flask for 16 hours under vacuum. After degassing, the curing agent and accelerator were added and the final mixture was speed mixed at 2100 rpm for 6 minutes.

Bidirectional dry glass plies $[0/90]_{12}$ with the nanorubber-toughened matrix and produced by hand lay-up were vacuum bagged and cured in an autoclave under a 6 atm pressure. Twelve and eight layers of glass plies were used for fracture toughness tests, Charpy impact tests and inter laminar shear strength (ILSS) tests, respectively. The composite panels were heated to 120°C at a heating rate of $0.5^{\circ}\text{C}/\text{min}$ and held for 1 hour at this temperature before cooling down to RT at the same rate, in an autoclave. The GFRP samples were cut from the cured panels using high-pressure water jet. The volume fraction of the glass fibres in the GFRP-composites was estimated using the following equation:

$$\%V_f = \frac{100W_{FAW}N_p}{B\rho_F} \quad (1)$$

Where W_{FAW} is the fibre areal weight, N_p is the number of plies, B is the thickness of the GFRP panels and ρ_F is the density of the glass fibre. The value of W_{FAW} is quoted from the manufacturer's datasheet of the glass fabrics, (287 g/m²). The density of the glass fibre is 2.54 g/cm³ [12]. The glass fibre volume fraction of the composites was 40±4%.

The scanning electron microscopy (SEM) studies on the fracture surface of the matrix showed that CNBR-NP was evenly distributed, however slight agglomeration existed in the X NBR-NP/ R formulations (Figure 1). In all the loadings a high amount of nanorubber de-bonding was observed, which resulted in nano and micro-voids formation in the composites. Further details on the processing and characterisation of these formulations can be found in [13].

3. CHARACTERISATION

The glass transition temperature of the GFRP was evaluated using a dynamic mechanical analyser DMA Q800, TA Instruments. Laminates with dimensions of 50×10×2 mm have been tested under three point bending loading and a fixed frequency of 1 Hz. Temperature ramps were carried out from 20 to 200°C at a heating rate of 2°C/min. The glass transition temperature was determined as the maximum stationary point of the tan δ vs. temperature curve. The data were obtained on an average of three samples.

For short beam shear (SBS) loading, samples with dimensions of 20×6.35×3.2 mm have been tested following the ASTM D2344 standard. The tests have been carried out using a Zwick Z250 universal testing machine at RT (23°C), with a crosshead speed of 1.3mm/min. The samples were placed on two rollers to allow a lateral adjustment and subjected to central loading at mid span. The span length (S) to specimen thickness (t) ratio was 5. The beams have been loaded until failure, and the failure load was used to calculate the apparent interlaminar shear strength (APS) of the composites. The failure load was interpreted as the first maximum load attained on load vs. crosshead displacement graphs. The APS was calculated as follows:

$$APS = \frac{0.75P_{max}}{wt} \quad (2)$$

Where P_{max} represents the breaking load, w the width of specimen and t the thickness of specimen. Five samples were tested from each configuration.

The effect of the nanorubber toughening on Mode I delamination (toughness G_{IC}), was studied using a double cantilever beam (DCB) test on GFRP samples following the EN6033 standard. Again, a Zwick Z250 tensile machine with a crosshead speed of 10mm/min was used for these tests. The samples were loaded perpendicular to the delamination surfaces.

A piece of release film (PTFE film) was placed on the mid plane of the stacked plies during the hand lay-up process to create a 30mm long pre-crack. Five DCB specimens with dimensions of 250×25×3 mm were tested for each matrix formulation. Screw-able grips were clamped onto the two faces of the specimen ends that featured the manufactured cracks. The edges of the specimens have been coated with white paint and

marked for a clear reading of the crack length. The pre-cracked samples were loaded until a total propagated crack length of approximately 100 mm was reached. The interlaminar fracture toughness energy was calculated from the propagated crack length and the applied energy determined from load-cross head displacement diagram. The interlaminar fracture toughness is calculated with the following formula:

$$G_{IC} = \left[\frac{A}{aw} \right] \times 10^6 \quad (3)$$

Where:

G_{IC} is the fracture toughness (J/m^2), A is the required energy to achieve the total propagated crack length (Joules), a is the crack length (mm) and w is the width of the specimen (mm).

Scanning electron microscopy (SEM) at secondary electron mode was used to study the fracture surfaces of the GFRP laminates. The samples were vacuum coated with gold using a sputter coater. Images were taken using an accelerating voltage of 20-25 keV with a magnification between 90 to 2000 times.

To study the Mode II interlaminar fracture toughness, samples with dimensions of 150×25×3 mm were tested at a crosshead speed of 1mm/min. The samples were positioned on a three-point bend fixture with a total span of 100 mm and an initial crack length of 34-35 mm. Five specimens for each epoxy configuration have been tested.

The samples were unloaded at the maximum load, and the mode II fracture toughness, G_{IIC} , was calculated at the maximum load sustained by the sample.

According to the protocol described in [14, 15]:

$$G_{IIC} = \frac{9000 P a^2 \delta}{2w \left[\frac{1}{4} L^3 + 3a^3 \right]} \quad (4)$$

In (4), P is the load (N), δ is the crosshead displacement at the crack growth onset (mm), w the specimen width (mm), a the initial crack length (mm) and L the span length (mm). Similarly to Mode I delamination, five samples have been tested corresponding to each epoxy composition. The experimental setups for the G_{IC} and G_{IIC} testing are shown in Figure 2.

For the Charpy impact tests, five samples from each epoxy batch were tested at RT (23°C) using a Hounsfield Balanced impact machine following the ASTM D 256 standard.

4. RESULTS AND DISCUSSIONS

The variation of the T_g with the nanorubber loading is given in Table 2. A 2°C decrease in the T_g can be observed when adding 20 phr of NBR-NP to the matrix, indicating the presence of a slightly less dense resin network. Almost no change in the T_g of the samples with the CNBR-NP modification indicates that almost all of the CNBR-NP phase is phase-separated [16]. Further details on the general behaviour of the T_g versus the nanorubber loading can be found in [13].

The apparent interlaminar shear strength, failure stresses and corresponding strains of the GFRP panels are presented in Table 3. For each laminate tested, a load-displacement

curve that represents the average of the five samples is shown in Figures 3 (a) and (b), respectively.

Laminates show a nearly linear elastic behaviour at the early stage of loading. This continues until an elastic limit is reached. After this point each laminate shows a decrease in load which is sudden in composites like GFRP with neat resin matrix. In the nanorubber-modified samples, the decrease in load is ductile and the crosshead displacement till fracture is larger. This increase in crosshead displacement is due to a decrease in the composite stiffness in nanorubber-modified samples, resulting in higher deflections at the same load levels.

The results show that, GFRP with neat R/ 1FS matrix achieved the highest peak load and the apparent interlaminar shear strength (APS) decreased continuously with rubber loading. The decrease in the APS values is attributed to the low strength and stiffness of the nanorubber particles decreasing the final strength and stiffness of the laminates.

The Mode I fracture toughness of the GFRP laminates based on an average of 5 samples are summarised in Table 4. There is a 190% and 150% increase in G_{IC} with 20 phr CNBR-NP and NBR-NP addition to the matrix, respectively.

Figures 4 (a) and (b) show the load vs. displacement curves of the GFRP samples with CNBR-NP and NBR-NP modified matrices, respectively. The maximum loads and displacements to fracture increase proportionally to the nanorubber concentration. Figure 4 also shows that the force linearly increases until it reaches the maximum force value, and then gradually decreases with zigzag shape during the propagation stages. This could be due to the variations of resin-rich or fibre-rich regions along the longitudinal directions [17, 18].

The fracture process was recorded by a video camera to analyse the crack initiation and propagation. In Figure 5 (a), it is possible to observe that the type of crack has a rather typical brittle topology, and no micro crack formation is observed in the GFRP panel with the R/ 1FS matrix. However, in the laminate with the 20 CNBR-NP/ R matrix a significant amount of micro crack formation has been observed, with the crack often deviating from its path (Figure 5 (b)). Such zig-zag propagating crack with branched paths requires a higher driving force and creates a larger fracture area, resulting therefore in higher fracture toughness. Hence, the enhanced interlaminar fracture toughness of the GFRP panels with nano-toughened matrices can be explained by the increased fracture surface area due to the crack deflection [17].

SEM over the fracture surfaces from the DCB samples has been used to evaluate the fibre-matrix interfacial bonding and the toughening mechanisms existing in the composites. In Figures 6 (a) and (b), the fracture surface of the composite panel with the unmodified epoxy matrix shows a typical brittle fracture with no plastic deformation. Figures 6 (c) and (d) shows the micrographs of the fracture surface of a laminate with 20 CNBR-NP/ R matrix, in which a high amount of nanorubber debonding can be observed to provide the toughening mechanism. In Figure 6 (f), it is possible to observe the initiation of an interesting interphase between the glass fibres and the NBR-NP modified matrix. The same interphase was however not observed in the CNBR-NP toughened laminates. High amount of fibre bridging responsible for the high interlaminar fracture toughness appears to exist in the two nanorubber-modified epoxy formulations. Due to good adherence of NBR-NP modified resin matrix to the glass fibre, tortuosity is observed in greater aspects, which was reflected in the mechanical properties as a higher G_{IIC} value. The toughening effect can be attributed to the inherent

tough and ductile properties of the nanorubbers themselves. It is proved with SEM that these properties of nanorubbers resulted in fibre bridging as well as nanorubber debonding.

The Mode II fracture toughness data of the GFRP samples obtained from the ENF specimens are presented in Table 5. Mode II interlaminar fracture energy values are higher than the Mode I ones because the crack propagation occurs in shear rather than tensile mode. It is possible to observe a strong dependency of the Mode II fracture toughness (G_{IIC}) on the fibre-matrix bonding. The increase in the G_{IIC} toughness with increasing nanorubber concentration can be explained by the enhanced bonding of the nanorubber toughened resin matrix to the glass fibres (see Figure 6). When the fiber-matrix bonding is strong, several energy absorbing phenomena such as matrix deformation, matrix cracking, fibre pull-out, and interfacial failure take place [19]. As a result of these phenomena, the G_{IIC} of the composites shows a significant improvement.

Figure 7 shows the corresponding load vs. displacement curves related to the ENF samples. The load increases until the crack initiates and propagates, which then results in a decrease in load. It can be seen that with an increase in nanorubber loadings, the maximum load attained before fracture and the displacement to failure both increase.

The Charpy impact strength data of the GFRP panels are given in Table 6. Addition of 20 phr of CNBR-NP or NBR-NP to the resin matrix resulted in this case in a 37% average decrease in the impact strength of the composites.

A composite with low interfacial strength has an inefficient transfer of energy from the matrix to the fibre, and as a result a lower energy is required for breaking. Moreover, the cracks formed in a composite with higher impact toughness tend to branch out. A

large number of cracks lead to a greater area of fracture and therefore a higher energy level is associated with the toughness of the composite. It is therefore justifiable that a composite with lower interfacial strength between the fibres and the matrix has higher impact strength values [20]. Thus, it is likely that the adhesion between the fibres and the matrix is enhanced with the increase of the nanorubber loading.

In Figure 8, the GFRP sample with the pristine matrix showed a high amount of delamination during fracture. However, delamination was hardly noticed in the other laminates with the nanorubber-modified matrices, confirming similar findings from other researchers [21, 22].

5. CONCLUSIONS

In the present study, nano-sized CNBR and NBR rubber particles have been used to improve the fracture toughness of GFRP composites. Special emphasis has been placed upon the evaluation of the fracture toughness of the nano-acrylonitrile butadiene rubber toughened epoxy composites under loading conditions corresponding to Modes I and II. The most efficient dispersion technique was evaluated and the mechanical and morphological properties of the glass fibre laminates produced with these nano-modified matrices have been analysed.

The fracture toughness of the GFRP laminates improved significantly with the nanorubber modification of the matrix, which was justified by the changed morphology of the resins. G_{IC} and G_{IIC} toughness of the GFRP panels were increased by 190% and 70% with rubber loading in both systems. The T_g was constant within the experimental error. The main toughening mechanisms were identified as fibre bridging, crack path deflection and nanorubber de-bonding. The elastomeric nature of the nanorubbers

caused a reduction in the interlaminar shear strength, indicating an enhancement in flexibility of the GFRP composites with the dispersion of the nanorubber.

ACKNOWLEDGEMENTS

The research leading to these results has received funding from the FP7-MC-ITN under grant agreement No. 264710. The authors would like to thank the Directorate-General for Science, Research and Development of the European Commission for financial support of the research. The authors from Kingston University London would like to thank Cytec Industrial Materials for their kind supply of the chemicals for the study.

REFERENCES

- [1] A. G. McKown, "Particulate adhesive containing polyepoxides, carboxylated butadiene-acrylonitrile copolymer and a urea derivative as a curing agent, United States patent office". Patent US3655818 A, 11 April 1972.
- [2] S.-G. Hong, "The curing behaviour and adhesion strength of the epoxidized natural rubber modified epoxy/dicyandiamide system," *Journal of Polymer research*, vol. 12, pp. 295-303, 2005.
- [3] Q. Wang , "Study of the isothermal curing of an epoxy prepreg by near-infrared spectroscopy," *Journal of applied polymer science*, vol. 87, no. 14, pp. 2295-2305, 2003.
- [4] S.-G. Hong, "The curing behaviour of the epoxy/dicyandiamide system modified with epoxidized natural rubber," *Thermochemica Acta*, vol. 417, pp. 99-106, 2004.
- [5] D. Kohli, "High performance adhesive compositions". Patent US20110048637 A1, 3 3 2011.
- [6] J. K. Fink, *Reactive polymers fundamentals and applications: A concise guide to industrial polymers*, Plastics Design Library, 2005.
- [7] H. Ma, G. Wei and Y. Liu, "Effect of elastomeric nanoparticles on properties of phenolic resin," *Polymer*, vol. 46, pp. 10568-10573, 2005.

- [8] H. C. Gardner and R. H. Newman-Evans, "Carboxylated rubber particles as tougheners for fiber reinforced composites". Patent US4977215 A, 11 12 1990.
- [9] H. Fan, Y. Liu and X. Zhang, "Effect of elastomeric nanoparticles on toughness and heat resistance of epoxy resins," *Macromolecular rapid communications*, vol. 23, pp. 786-790, 2002.
- [10] H. Fan, Y. Liu, X. Zhang, J. Gao, Z. Song, B. Tang, G. Wei and J. Qiao, "Interface and properties of epoxy resin modified by elastomeric nano-particles," *Science China Chemistry*, vol. 48, no. 2, pp. 148-155, 2005.
- [11] T. Hsieh, A. Kinloch, K. Masania, L. John, A. Taylor and S. Sprenger, "The toughness of epoxy polymers and fibre composites modified with rubber microparticles and silica nanoparticles," *Journal of materials science*, vol. 45, pp. 1193-1210, 2010.
- [12] "Hexcel technical fabrics handbook," Texas, 2010.
- [13] N. G. Ozdemir, T. Zhang, H. Hadavinia, I. Aspin and J. Wang, "Rheological properties, cure characteristics, and morphology of acrylonitrile-based nanorubber modified epoxy," *Journal of applied polymer science*, 2015.
- [14] *Protocol for interlaminar fracture testing No.2, Mode II (ENF)*, 1992.
- [15] R. F. Gibson, in *Principles of composite materials mechanics*, McGraw Hill, USA, 1994, pp. 395-397.
- [16] J. K. Kim and S. Datta, "Rubber-Thermoset Blends: Micro and Nano Structured," in *Advances in elastomers I*, Springer Berlin Heidelberg, 2013, pp. pp 229-262.
- [17] N. A. Siddiqui, R. S. Woo, J.-K. Kim, C. C. Leung and M. Arshad, "Mode-I interlaminar fracture behaviour and mechanical properties of CFRPs with nanoclay-filled epoxy matrix," *Composite Part A*, vol. 38, pp. 449-460, 2007.
- [18] H. M. Grabr, A. M. Elrahamn, K. Okubo and T. Fujii, "Interfacial adhesion improvement of plain woven carbon fiber reinforced epoxy filled with micro-fibrillated cellulose by addition of liquid rubber," *Journal of materials science*, vol. 45, pp. 3841-3850, 2010.
- [19] R. Bagheri, B. T. Marouf and R. A. Pearson, "Rubber toughened epoxies - A Critical Review," *Polymer Reviews*, vol. 49, no. 3, pp. 201-225, 2009.
- [20] S. N. Monteiro, "Processing and properties of continuous and aligned curaua fibers incorporated polyester composites," *Journal of materials research technology*, vol.

2, no. 1, pp. 2-9, 2013.

- [21] G. Escamilla, "Flexural, impact and compressive properties of a rigid-thermoplastic matrix/cellulose fibre reinforced composites," *Composites Part A*, vol. 33, no. 4, p. 539–549, 2002.
- [22] P. Wambua, "Natural fibres: can they replace glass in fibre reinforced plastics?," *Composites Science and Technology*, vol. 63, no. 9, p. 1259–1264, 2003.

Figure Captions

Figure 1. SEM images of the fracture surfaces of (a) R/ 1FS, (b) 20CNBR-NP/ R, (c) 20NBR-NP/ R

Figure 2. Experimental apparatus of (a) DCB test, (b) ENF test

Figure 3. Loads vs. displacements for the GFRP panels with (a) X CNBR-NP/ R matrix, (b) X NBR-NP/ R matrix

Figure 4. Load vs. displacement curves of GFRP tested with DCB (a) X CNBR-NP/ R matrix, (b) X NBR-NP/ R matrix

Figure 5. Propagating cracks during the DCB test, (a) GFRP with R/ 1FS matrix, (b) GFRP with 20 CNBR-NP/ R matrix

Figure 6. SEM images of the fracture surfaces of (a), (b) laminate with R/ 1FS matrix, (c), (d) laminate with 20 CNBR-NP/ R matrix, (e), (f) laminate with 20 NBR-NP/ R matrix

Figure 7. Force vs. deformation for (a) GFRP with X CNBR-NP/ R matrices, 1: R/1FS, 2: 5CNBR-NP/ R, 3: 10CNBR-NP/ R, 4: 15CNBR-NP/ R, 5: 20CNBR-NP/ R (b) GFRP with X NBR-NP/ R matrices, 1: R/1FS, 2: 5NBR-NP/ R, 3: 10NBR-NP/ R, 4: 15NBR-NP/ R, 5: 20NBR-NP/ R

Figure 8. GFRP with nanorubber-toughened matrices show less delamination during fracture

Table Captions

Table 1. Formulations of the epoxy used in this work in phr (parts per hundred of DGEBA)

Table 2. Glass transition temperature (T_g) of the GFRP samples

Table 3. Apparent interlaminar shear strength of the GFRP samples, σ = standard deviation, s = Crosshead displacement at fracture, V_f = Volume fraction of the glass fibres in the composites

Table 4. G_{IC} Test data of the GFRP panels, σ = Standard Deviation

Table 5. G_{IIC} Test data, σ = Standard Deviation

Table 6. Charpy impact test data, σ = Standard Deviation

Table 1. Formulations of the epoxy used in this work in phr (parts per hundred of DGEBA)

CODE	DGEBA	DICY	Diurone	NBR-NP	CNBR-NP	Fumed Silica
R	100	14	6	-	-	-
R/ X FS	100	14	6	-	-	X
X CNBR-NP/ R	100	14	6	-	X	-
X NBR-NP/ R	100	14	6	X	-	-

Table 2. Glass transition temperature (T_g) of the GFRP samples

X (NP phr)	X CNBR-NP/ R		X NBR-NP/ R	
	T_g (°C)	σ (°C)	T_g (°C)	σ (°C)
0 (1 FS)	140	0.1	140	0.0
5	143	0.2	140	0.0
10	142	0.1	139	0.6
15	141	0.0	140	0.1
20	140	0.0	138	0.8

Table 3. Apparent interlaminar shear strength of the GFRP samples, σ = standard deviation, s = Crosshead displacement at fracture, V_f = Volume fraction of the glass fibres in the composites

X (NP phr)	X CNBR-NP/ R				X NBR-NP/ R			
	APS (MPa)	σ (MPa)	s (mm)	V_f	APS (MPa)	σ (MPa)	s (mm)	V_f
0 (1 FS)	70	0.7	0.6	0.40	70	0.7	0.6	0.40
5	68	0.4	0.7	0.38	69	0.5	0.7	0.38
10	63	0.8	0.7	0.38	63	0.4	0.8	0.37
15	61	0.2	0.8	0.38	57	0.1	0.8	0.39
20	56	0.4	0.9	0.36	54	0.8	0.9	0.38

Table 4. G_{IC} Test data of the GFRP panels, σ = Standard Deviation

X (phr)	X CNBR-NP/ R			X NBR-NP/ R		
	G_{IC} (J/m²)	σ (J/m²)	% Increase	G_{IC} (J/m²)	σ (J/m²)	% Increase
0 (1 FS)	441	22	-	441	22	-
5	741	13	68	705	54	60
10	860	33	95	887	16	101
15	1042	20	136	977	42	122
20	1277	17	190	1103	52	150

Table 5. G_{IIC} Test data, σ = Standard Deviation

X (phr)	X CNBR-NP/ R			X NBR-NP/ R		
	G_{IIC} (J/m²)	σ (J/m²)	% Increase	G_{IIC} (J/m²)	σ (J/m²)	% Increase
0 (1 FS)	2678	153	-	2678	153	-
5	3796	53	42	3884	297	45
10	3461	61	29	4475	430	67
15	3838	303	43	3407	206	27
20	4637	397	73	3830	250	43

Table 6. Charpy impact test data, σ = Standard Deviation

X (phr)	X CNBR-NP/ R			X NBR-NP/ R		
	σ_c (kJ/m²)	σ (kJ/m²)	% Decrease	σ_c (kJ/m²)	σ (kJ/m²)	% Decrease
0 (1 FS)	185	12	-	185	12	-
5	141	9	24	144	7	22
10	135	5	27	136	6	26
15	127	7	31	126	7	32
20	116	11	37	118	4	36

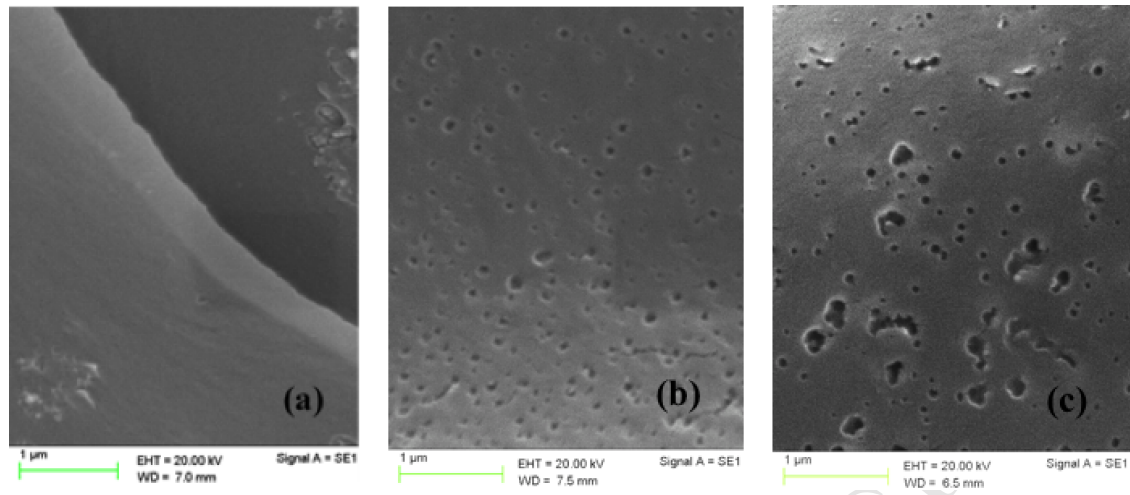


Figure 1. SEM images of the fracture surfaces of (a) R/ 1FS, (b) 20CNBR-NP/ R, (c) 20NBR-NP/ R

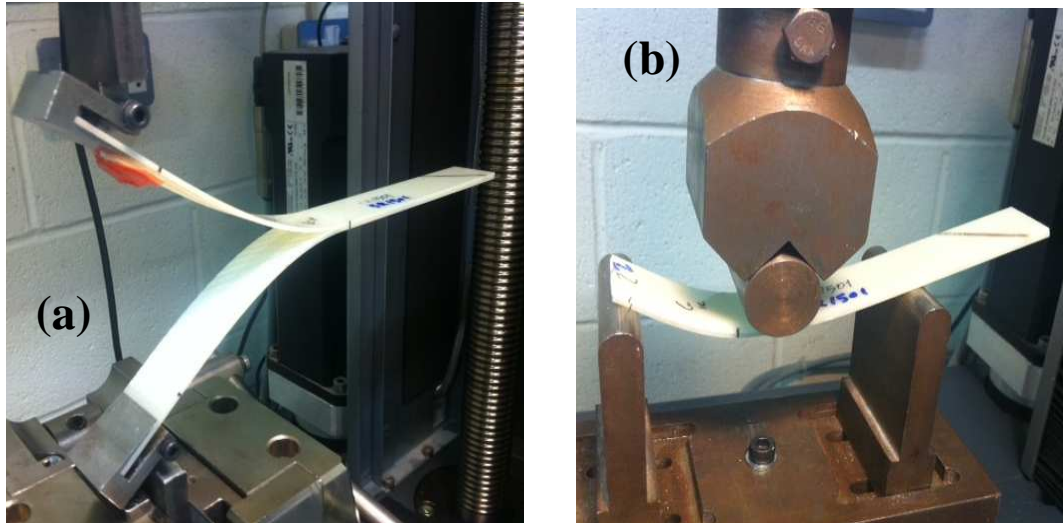


Figure 2. Experimental apparatus of (a) DCB test, (b) ENF test

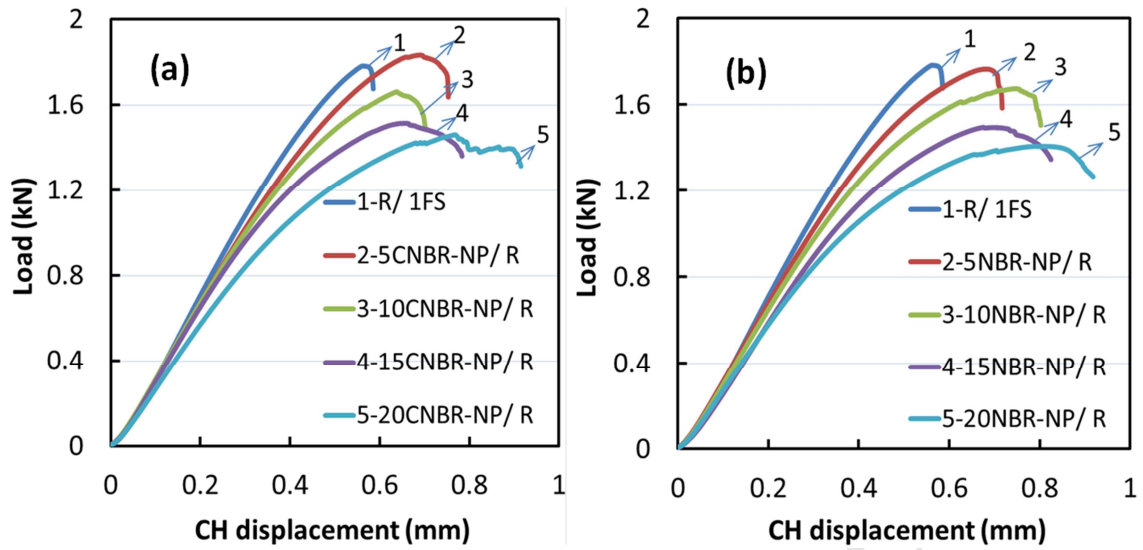


Figure 3. Loads vs. displacements for the GFRP panels with (a) X CNBR-NP/ R matrix, (b) X NBR-NP/ R matrix

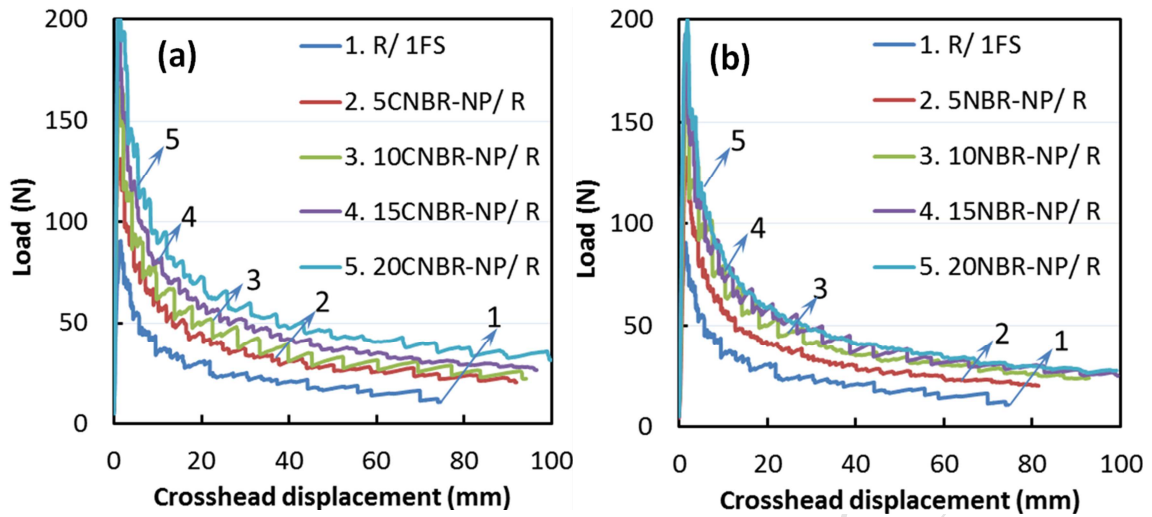


Figure 4. Load vs. displacement curves of GFRP tested with DCB (a) X CNBR-NP/ R matrix, (b) X NBR-NP/ R matrix

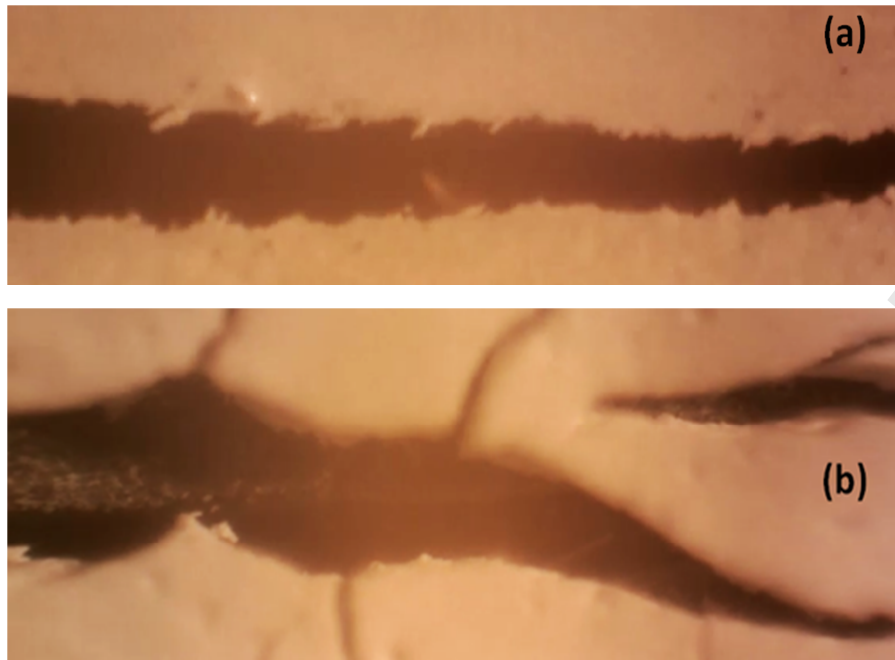


Figure 5. Propagating cracks during the DCB test, (a) GFRP with R/ 1FS matrix, (b) GFRP with 20 CNBR-NP/ R matrix

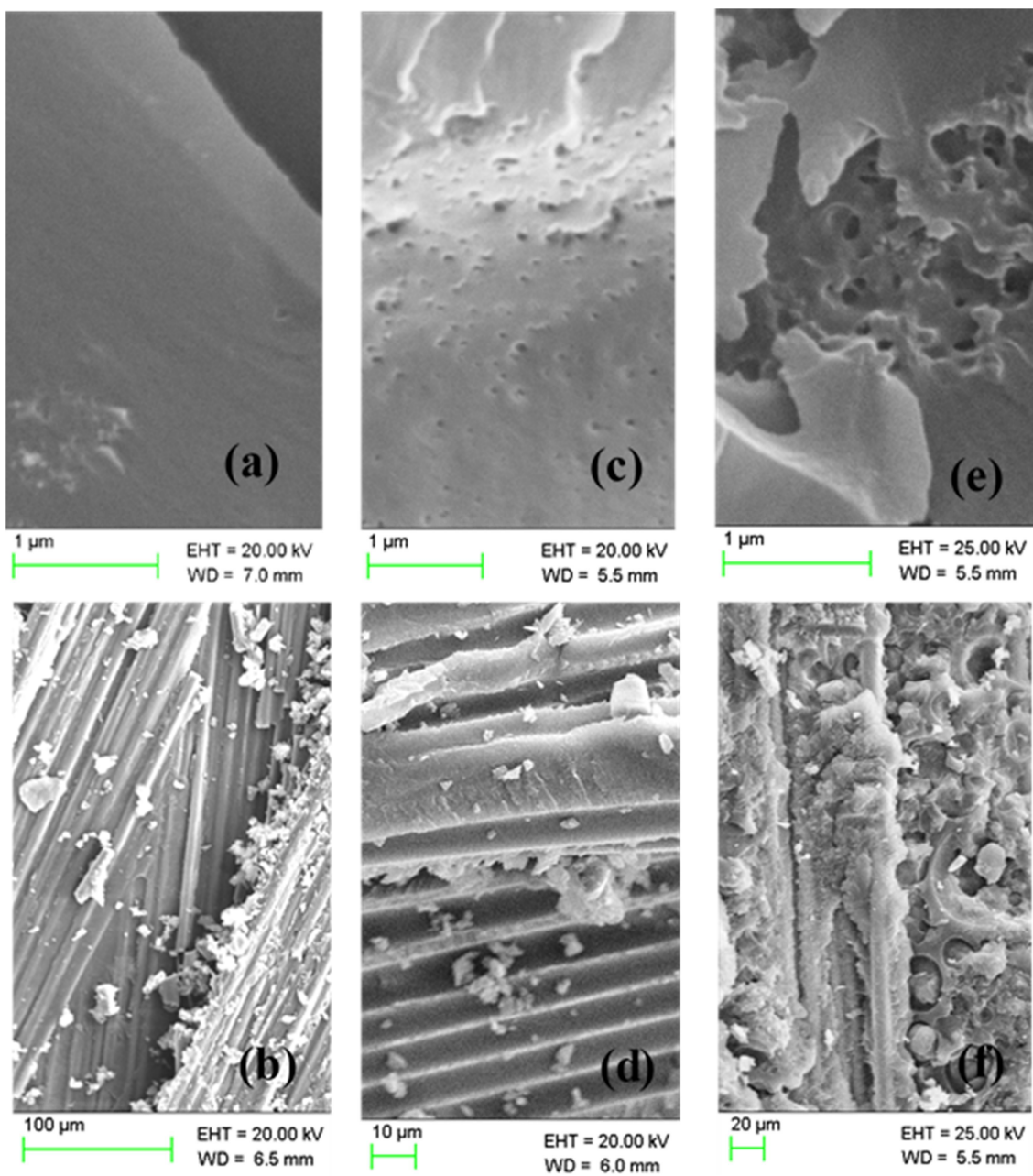


Figure 6. SEM images of the fracture surfaces of (a), (b) laminate with R/ 1FS matrix, (c), (d) laminate with 20 CNBR-NP/ R matrix, (e), (f) laminate with 20 NBR-NP/ R matrix

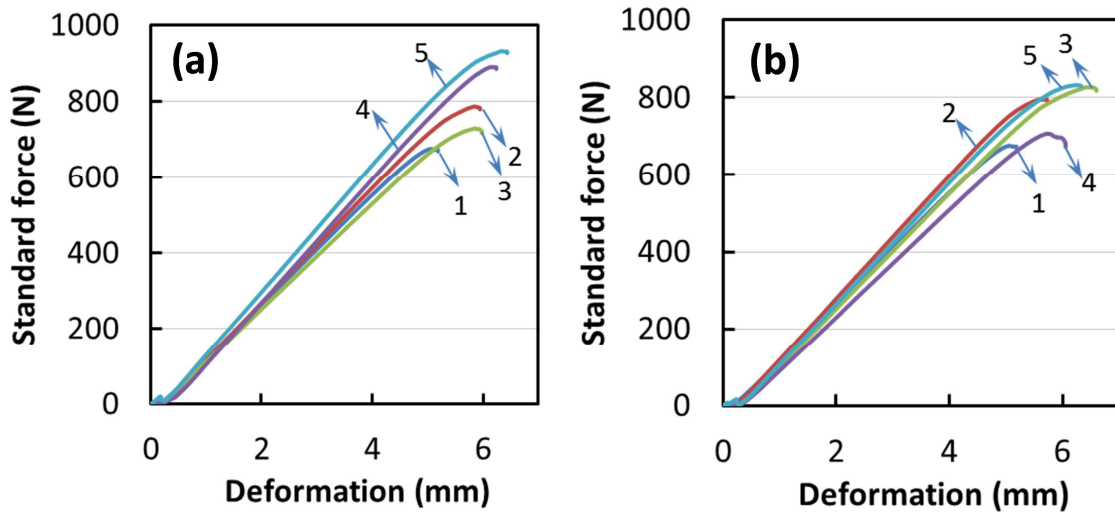
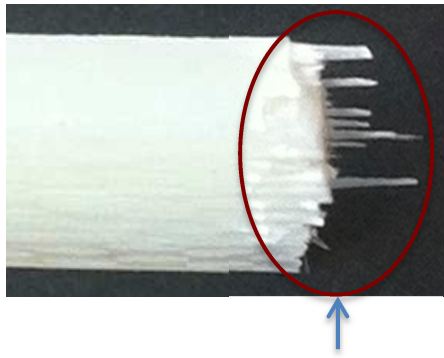
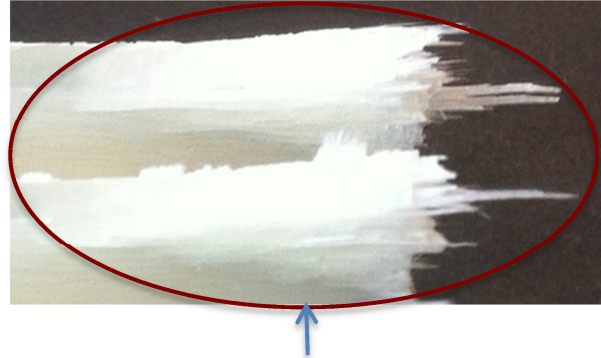


Figure 7. Force vs. deformation for (a) GFRP with X CNBR-NP/ R matrices, 1: R/1FS, 2: 5CNBR-NP/ R, 3: 10CNBR-NP/ R, 4: 15CNBR-NP/ R, 5: 20CNBR-NP/ R (b) GFRP with X NBR-NP/ R matrices, 1: R/1FS, 2: 5NBR-NP/ R, 3: 10NBR-NP/ R, 4: 15NBR-NP/ R, 5: 20NBR-NP/ R



Delamination zone, GFRP with
20CNBR-NP/ R matrix



Delamination zone, GFRP with R/ 1FS
matrix

Figure 8. GFRP with nanorubber-toughened matrices show less delamination during fracture